Low-Complexity Multi-tap ET-DFE-PU for Soft-Input FEC in High-Speed IM/DD systems

Xue Zhao, Jiahao Zhou, Jing Zhang*, Rui Wang, Zhengyu Ma, Shaohua Hu, Bo Xu and Kun Qiu
Key Lab. of Optical Fiber Sensing and Communications, University of Electronic Science and Technology of China, Chengdu 611731, China
zhangjing1983@uestc.edu.cn

Abstract: We propose a low-complexity multi-tap LUT-based ET-DFE-PU algorithm to alleviate the degradation on LLR by error propagation. The experimental results show that the proposed algorithm can achieve 3.4-dB receiver sensitivity improvement compared with conventional DFE.

1. Introduction

Driven by large bandwidth internet applications such as media service, cloud computing and the Internet of Things (IoT), there is an exponential increasing requirement of data traffic in data center interconnects (DCIs). The intensity modulation and direct-detection (IM/DD) system with 4-level pulse amplitude modulation (PAM-4) modulation is considered as an effective solution in short-reach applications due to its low cost, power consumption and computational complexity [1]. Band-limited effect and signal-to-signal beating interference are two limitations for IM/DD systems. Feed-forward equalizer (FFE) combined with decision feedback equalizer (DFE) can effectively compensate for linear and nonlinear distortions with lower complexity [2]. However, the compensation of large inter-symbol interference (ISI) caused by severe bandwidth limitation and chromatic dispersion has become extremely challenging as the increasing of data rate [3]. Forward error correction (FEC), as a cost-effective method to provide additional code gain, has been widely employed to improve overall performance and guarantee reliable transmission [4]. However, the error propagation resulted from DFE significantly degrades the log-likelihood ratio (LLR) distribution and the soft-decision forward error correction (SD-FEC) decoding performance. A weighted DFE (WDFE) that introduces a reliability value to control the weight of feedback symbols has been studied to suppress the burst error propagation [5]. However, the WDFE cannot fully compensate for the spectral nulls because only a part of feedback symbols are directly decided. In addition, the interleaving or precoding technique at the transmitter side can suppress the burst errors of DFE [6, 7]. However, the implementation of interleaving and deinterleaving increases the latency. While the precoding needs to adopt the quantized LLRs for decoding. This degrades the SD-FEC decoding performance. Except for the error propagation problem, the time consuming of feedback of DFE also limit its application in high-speed transmissions. Partially unrolling architecture is well-known to relax the timing consuming constraints [8]. It can compress the possible state for each symbol and reduce the implementation complexity.

In this paper, we propose a multi-tap look-up-table (LUT)-based error-tracking DFE with partially unrolling (ET-DFE-PU) to alleviate the degradation on LLR by error propagation resulted from DFE. In ET-DFE, we use an error tracking model to calculate the error-offset probabilities of DFE so that the distorted LLRs can be corrected. Thus, the performance of post-FEC BER is improved with more accurate LLR. To reduce the calculation complexity of LLRs, we establish a LUT to record the indexing symbol and its corresponding probability. Moreover, a low-complexity partially unrolling architecture is used to reduce possible output states. The proposed algorithm is verified in a 170-Gb/s PAM-4 signal IM/DD system at C-band. The experiment results show that the LUT-based ET-DFE-PU can effectively solve the error propagation problem of DFE in SD-FEC decoding stage. The proposed ET-DFE-PU achieves a 3.4-dB receiver sensitivity gain compared with conventional DFE after decoding.

2. Principle of multi-tap LUT-based ET-DFE-PU

Figure 1(a) shows the block diagram of the multi-tap ET-DFE. In Fig. 1(a), a post filter (PF) is used to suppress the noise enhancement caused by FFE, and the *N*-tap DFE cancels the trailing ISI resulted from PF. The DFE equalized symbol $\bar{y}_i$ at time *i* can be described as,

$$\bar{y}_i = y_i - \sum_{k=1}^{N} b_k d_{i-k} = x_i + \sum_{k=1}^{N} b_k x_{i-k} + n_i - \sum_{k=1}^{N} b_k d_{i-k} = x_i + n_i + \sum_{k=1}^{N} b_k e_{i-k} = d_i + e_i + n_i + \sum_{k=1}^{N} b_k e_{i-k} \quad (1)$$

where y_i is the signal after PF, x_i is the original PAM-*M* symbol belonging to $\{\pm 1, \pm 3, \ldots, \pm(\mathrm{M}-1)\}$, b_k is tap coefficient of DFE. The n_i stands for the additive white gaussian noise (AWGN) with noise variance of δ^2, and d_i is the hard decision of $\bar{y}_i$. The error produced by DFE is $e_i = x_i - d_i$. We only consider 0 and ±2 for error events, and neglect errors like ±4 and ±6, which would only occur in lower signal-to-noise ratio (SNR) case. We define the biased state of the output symbol as $s_i \in S = \{l, c, r\}$, which corresponding to $e_i \in \{+2, 0, -2\}$. We use $\boldsymbol{P}_i$ to record different

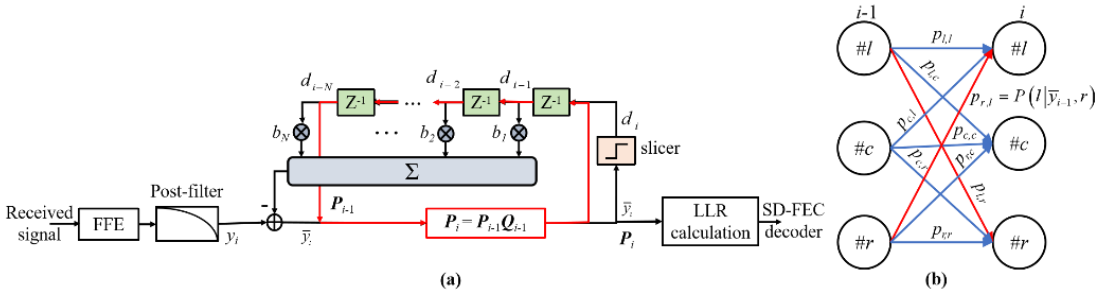

Fig. 1. (a) Block diagram of ET-DFE. (b) The error tracking model of DFE.

biased states probabilities conditioned on the previous equalized symbol, where $\boldsymbol{P}_i = [P(s_i|\bar{y}_{i-1}, \bar{y}_{i-2}, \ldots)]$, and $\boldsymbol{P}_i$ is initialized to [0, 1, 0]. Fig. 1(b) shows the error tracking model of DFE. In Fig. 1(b), $p_{r,l}$ indicates the state transition probability from error state *r* to *l*. According to the error tracking model, we create a transition probability matrix $\boldsymbol{Q}_i$. Then, the $\boldsymbol{P}_{i+1}$ can be calculated by recursive formulate as $\boldsymbol{P}_{i+1} = \boldsymbol{P}_i \boldsymbol{Q}_i$. $\boldsymbol{Q}_i$ is obtained by a row normalization on $\boldsymbol{W}_i$. According to Eq. (1), we define an offset Δ and assume $\bar{y}_i \sim N(d_i + \Delta, \delta^2)$. The probability density function (PDF) is denoted by $f(\cdot)$. Then, $\boldsymbol{W}_i$ can be calculated as:

$$\boldsymbol{W}_i = \begin{bmatrix} p_{l,l} & p_{l,c} & p_{l,r} \\ p_{c,l} & p_{c,c} & p_{c,r} \\ p_{r,l} & p_{r,c} & p_{r,r} \end{bmatrix} = \begin{bmatrix} \sum_{m\in\{\boldsymbol{U}_i(v)>0\}} f(2+m) & \sum_{m\in\{\boldsymbol{U}_i(v)>0\}} f(m) & \sum_{m\in\{\boldsymbol{U}_i(v)>0\}} f(-2+m) \\ f(2) & f(0) & f(-2) \\ \sum_{z\in\{\boldsymbol{U}_i(v)<0\}} f(2+z) & \sum_{z\in\{\boldsymbol{U}_i(v)<0\}} f(z) & \sum_{z\in\{\boldsymbol{U}_i(v)<0\}} f(-2+z) \end{bmatrix} \tag{2}$$

$$where\ \boldsymbol{U}_i(v) = \sum_{k=1}^{N} b_k e_{i-k}, e \in \{+2, 0, -2\}, v = 0, 1, .., 3^N, \text{and } f(\triangle) = \frac{1}{\sqrt{2\pi}\delta} e^{-\frac{[\bar{y}-(d+\triangle)]^2}{2\delta^2}}$$

When d_i=(M–1) or -(M–1), the left or the right column of $\boldsymbol{W}_i$ is set to a zero column vector. In order to obtain more accurate LLRs, we introduce different offset states probabilities into the LLR calculation formula as,

$$\Lambda_j^S = \log \frac{\sum_{x\in\chi_j^0} \sum_{s\in S} f_{\bar{Y}|X,S}(\bar{y}|x,s) P(s|\bar{\mathbf{y}})}{\sum_{x\in\chi_j^1} \sum_{s\in S} f_{\bar{Y}|X,S}(\bar{y}|x,s) P(s|\bar{\mathbf{y}})} \tag{3}$$

where j=1,2,…,log2(M), χ_j^0 and χ_j^1 are the sets of PAM-M symbols whose j-th bit is '0' and '1', respectively. $f_{\bar{Y}|X,S}(\bar{y}|x,s)$ is derived by $\bar{y} \sim N(x + \Delta, \delta^2)$, where Δ can be obtained from Eq. (1). The above PDF calculation leads to a significant increase in the computational complexity. We establish a PDF LUT to reduce the computation complexity of ET-DFE. We divide the continuous interval into a series of segments with the intervals of ΔI. The received signal is quantized by the center point of the segment. Then, the probability corresponding to the center point is stored in the LUT. The LUT is indexed by the training symbols, and its entries record the indexing symbol and the corresponding probability. For high-speed transmissions, we combine ET-DFE with low-complexity partially unrolling architecture to relax the timing constraints resulted by feedback of DFE [8]. The ET-DFE-PU employs a threshold detector to make a pre-decision at the output of FFE so that the possible states for each symbol are reduced from M to P, where M is the modulation level and N is the tap number of DFE [9]. Thus, the number of possible output cases is reduced from M^N to P^N.

3. Experiment investigation and results discussion

The experimental setup is illustrated in Fig. 2. A pseudo-random bit sequence (PRBS) is encoded by the LDPC code with block length of 64800 bits and code rate of 0.83. The encoded bit-streams are mapped into PAM-4 symbols. Then the data sequence is loaded into the arbitrary waveform generator (AWG) operating at 120 GSa/s. The generated PAM-4 signal passes through an electrical amplifier (EA) and then inputs to a 40-GHz Mach-Zehnder modulator (MZM). The laser is operated at 1550 nm with an output power of 12 dBm. After 5-km SSMF transmission, we use a boost amplifier (BA) to boost the optical signal since the photodiode (PD) is without a trans-impedance amplifier (TIA). Then, the variable optical attenuator (VOA) is adopted to adjust the receive optical power (ROP) of the TIA-free single-ended 40-GHz photodiode (PD) with maximum optical input power of 10 dBm. Finally, the detected electrical signal is sampled by a 59-GHz a real-time oscilloscope (RTO) operating at 256 GSa/s. Subsequently, the received signal is processed offline. The receiver DSP includes re-sampling, matched filter, equalization, PAM-4 de-

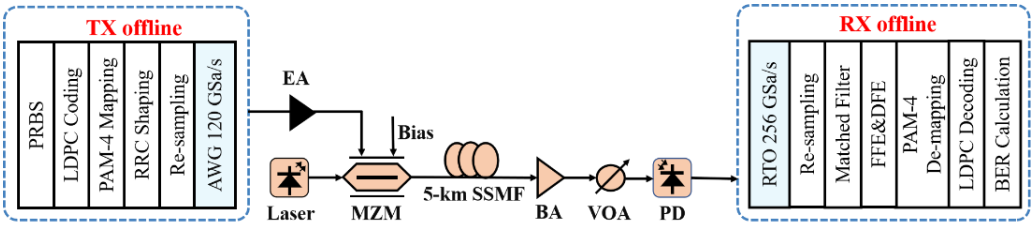

Fig. 2. Experimental setup of PAM-4 IM-DD system.

mapping, LDPC decoding and bit error ratio (BER) calculation. We compare the conventional DFE and the proposed ET-DFE-PU.

Fig. 3(a) shows the post-FEC BER performance of LUT-based ET-DFE-PU for 170-Gb/s PAM-4 signal transmission at a ROP of 10 dBm. In Fig. 3(a), the BER is floor and approximates the performance of conventional ET-DFE-PU when ΔI is set to 0.06. Fig. 3(b) shows the pre-FEC BER versus different ROPs. Both of DFE and LUT-based ET-DFE-PU are cascaded by a 181-tap FFE. The inset of Fig. 3(b) shows the amplitude histograms of PAM-4 signal after FFE at a ROP of 10 dBm, in which the signal cannot be distinguished. Therefore, we limit the set of most likely symbols for each time slot from four to three in ET-DFE-PU. In Fig. 3(b), the proposed LUT-based ET-DFE-PU outperforms conventional DFE by 0.2-dB gains in ROP at a BER of 2×10^{-2} due to the improved LLR accuracy. Fig. 3(c) shows the post-FEC BER versus different ROPs. The decoder utilizes belief propagation (BP) with 6 iterations. For the SD-FEC, the quality of LLR strongly affects the decoding performance. The proposed ET-DFE-PU can track DFE error propagation, and introduce the error information into the LLR calculation. Therefore, the LUT-based ET-DFE-PU can achieve 3.4-dB receiver sensitivity improvement at a BER of 6.35×10^{-3} compared with the conventional DFE. Fig. 3(d) shows the LDPC performance for DFE and LUT-based ET-DFE-PU. In Fig. 3(d), employing LUT-based ET-DFE-PU can decrease the post-FEC BER by more than one orders of magnitude compared to conventional DFE with the same pre-FEC BER. Besides, the required post-FEC BER increases from 2×10^{-2} for conventional DFE to 3.13×10^{-2} for LUT-based ET-DFE-PU at the pre-FEC BER of 1×10^{-2}, which can be translated to ~2.9-dB gains in ROP from Fig. 3(b).

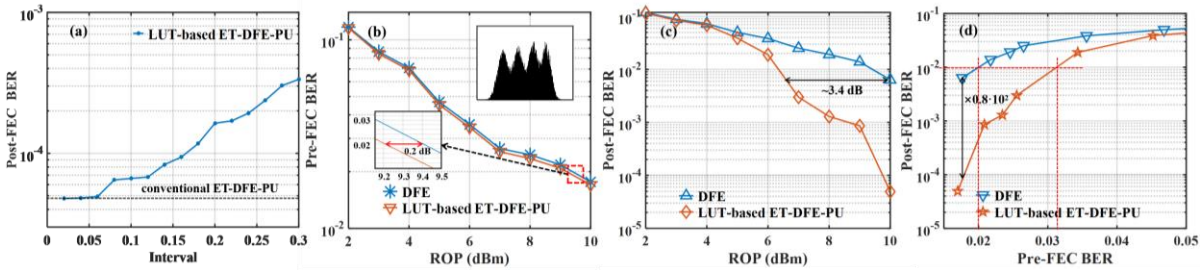

Fig. 3. (a) Post-FEC BER performance of LUT-based ET-DFE-PU. (b) Pre-FEC BER performance versus different ROPs. (c) Post-FEC BER performance versus different ROPs. (d) LDPC performance for DFE and LUT-based ET-DFE-PU.

4. Conclusions

In this paper, we have proposed a low-complexity LUT-based ET-DFE-PU for C-band PAM4 IM/DD system to improve the LLR accuracy. The experimental results show that the proposed ET-DFE-PU can achieve 3.4-dB receiver sensitivity improvement with the same post-FEC BER.

5. References

[1] X. Tang, S. Liu, Z. Sun, H. Cui, X. Xu, J. Qi, M. Guo, Y. Lu and Y. Qiao, Opt. Express **27**(18), 25708-25717 (2019).
[2] X. Wu, J. Zhang, A. P. T. Lau and C. Lu, Opt. Lett. **47**(6), 1565-1568 (2022).
[3] M. Xiang, S. Fu, O. Xu, J. Li, D. Peng, Z. Gao, Y. Wang and Y. Qin, J. Lightwave Technol. **40**(4), 987-996 (2022).
[4] T. Sugihara, T. Yoshida and T. Mizuochi, in OFC 2013, pp. OM2B.3.
[5] J. Zhou, C. Yang, D. Wang, Q. Sui, H. Wang, S. Gao, Y. Feng, W. Liu, Y. Yan, J. Li, C. Yu, and Z. Li, J. Lightwave Technol. **39**(4), 4601-4606 (2021).
[6] X. Liu, A. Shen, N. Cheng, Y. Luo, and F. Effenberger, in OFC 2021, pp. M3G.6.
[7] A. Mahadevan, D. Veen, N. Kaneda, A. Duque, A. Wijngaarden, and V. Houtsma, J. Opt. Commun. Netw. **13**(1), A100-A110 (2021).
[8] S. Kiran, S. Cai, Y. Luo, S. Hoyos and S. Palermo, IEEE Journal of Solid-State Circuits **54**(3), 659-671 (2019).
[9] J. Zhou, J. Zhang, X. Zhao, T. Jin, S. Hu, H. Lin, Z. Yu, Q. Zhang, B. Xu and K. Qiu, Opt. Express **30**(21), 37416-37425 (2022).
This work was supported by National Science Foundation of China (NSFC) (62301128 and 62111530150), and Fundamental Research Funds for the Central Universities (ZYGX2020ZB043 and ZYGX2019J008).